neat Fermat and dual-Archimedean yarns having about the same diameter and bias angle (fig. S2).

Diverse structural effects can potentially contribute to tensile actuation for coiled, two-end–tethered, nonplied yarns, including conversion between twist and writhe (in both uncoiled and coiled regions) and changes in coil diameter, pitch, and yarn length. Although twist-to-writhe conversion (corresponding to an increase in number of coils) would enhance thermal contraction during actuation, optical microscopy indicates that total coil number does not measurably increase during actuation for either heavily or lightly coiled, wax-filled, dual-Archimedean yarns. These results suggest that tensile contraction is predominantly caused by a decrease in separation between neighboring coils.

Yarn coiling increases the negative thermal expansion of a neat twist-spun yarn by a factor of ~10. Because these coiled neat yarns provide up to 7.3% hysteresis-free contraction when lifting heavy loads using temperature changes up to ~2560°C (Fig. 2B and movie S4), these muscles can be deployed in inert atmosphere to temperatures at which no other high–work-capacity actuator can survive.

For applications in which yarn-size torsional and tensile actuators are needed, the absence of electrolyte and associated packaging, the low required voltages, and the high cycle life and energy and power densities suggest the possibility of early commercial deployment. The main competing technology of NiTi shape memory metal actuators provides highly hysteretic actuator strokes; actuator control is complicated by the dependence of stroke on prior history within a cycle (*26*). This history dependence is small for the wax hybrid yarn results of Fig. 2A and should be negligible for cycling a neat yarn or any wax-filled yarn between molten states. However, as with shape memory metal wires and other thermally powered actuators (*26*), electrothermal energy conversion efficiency is low. Future possibilities include environmentally powered hybrid muscles that open textile pores or close window blinds when it is too hot, or actuate in response to agents in the environment.

References and Notes

1. T. Mirfakhrai *et al.*, *Smart Mater. Struct.* **16**, S243 (2007).
2. J. Foroughi *et al.*, *Science* **334**, 494 (2011).
3. P. Miaudet *et al.*, *Science* **318**, 1294 (2007).
4. A. T. Sellinger, D. H. Wang, L.-S. Tan, R. A. Vaia, *Adv. Mater. (Deerfield Beach Fla.)* **22**, 3430 (2010).
5. L. Chen *et al.*, *ACS Nano* **5**, 1588 (2011).
6. Y. Hu, W. Chen, L. H. Lu, J. H. Liu, C. R. Chang, *ACS Nano* **4**, 3498 (2010).
7. M. Zhang, K. R. Atkinson, R. H. Baughman, *Science* **306**, 1358 (2004).
8. M. Zhang *et al.*, *Science* **309**, 1215 (2005).
9. X. Zhang *et al.*, *Adv. Mater.* **18**, 1505 (2006).
10. Q. Li *et al.*, *Adv. Mater.* **18**, 3160 (2006).
11. X. Zhang *et al.*, *Small* **3**, 244 (2007).
12. L. Xiao *et al.*, *Appl. Phys. Lett.* **92**, 153108 (2008).
13. Y. Nakayama, *Jpn. J. Appl. Phys.* **47**, 8149 (2008).
14. M. B. Jakubinek *et al.*, *Carbon* **50**, 244 (2012).
15. M. D. Lima *et al.*, *Science* **331**, 51 (2011).
16. Materials and methods are available as supplementary materials on *Science* Online.
17. F. B. Fuller, *Proc. Natl. Acad. Sci. U.S.A.* **68**, 815 (1971).
18. A. Goriely, M. Tabor, *Physica D* **105**, 20 (1997).
19. A. F. da Fonseca, C. P. Malta, D. S. Galvão, *J. Appl. Phys.* **99**, 094310 (2006).
20. Y. Shang *et al.*, *Adv. Mater.* **24**, 2896 (2012).
21. The presently used term "inserted twist" (which is sometimes called linking number) is the sum of internal yarn twist and the twist due to coiling. As done for other structural terms, "yarn diameter" refers to the diameter of the component yarn even when it is within a coiled or plied structure, and is thereby differentiated from the "coiled yarn diameter" or the "plied yarn diameter."
22. E. T. Carlen, C. H. Mastrangelo, *J. Microelectromech. Syst.* **11**, 165 (2002).
23. R. K. Josephson, *Annu. Rev. Physiol.* **55**, 527 (1993).
24. D. R. Peterson, J. D. Bronzino, *Biomechanics: Principles and Applications* (CRC Press, Boca Raton, FL, 2008).
25. This efficiency was measured in the Fig. 1A configuration for 1.5% actuation of a coiled, wax-filled, 150-μm-diameter, dual-Archimedean yarn using a 1-ms electrical pulse and 55-MPa applied stress. Full contraction occurred within ~30 ms of pulse start.
26. J. E. Huber, N. A. Fleck, M. F. Ashby, *Proc. R. Soc. Lond. A* **453**, 2185 (1997).
27. To understand this conversion of yarn twist to twist due to yarn plying, overtwist a yarn and fold it back on itself. The yarn will automatically become two ply as the initial inserted twist is partially converted to plying in the opposite twist direction.
28. H. Peng *et al.*, *Nat. Nanotechnol.* **4**, 738 (2009).
29. M. Mizumoto, T. Ohgai, A. Kagawa, *J. Alloy. Comp.* **482**, 416 (2009).
30. P. Pötschke, S. Pegel, M. Claes, D. Bonduel, *Macromol. Rapid Commun.* **29**, 244 (2008).
31. R. Zhou *et al.*, *Nanotechnology* **21**, 345701 (2010).
32. B. T. Kelley, *Carbon* **29**, 721 (1991).

Acknowledgments: We thank X. Lepró for scanning electron micrograph (SEM) images of yarn cross sections; B. J. Swedlove, D. B. Hagenasr, J. M. Cruciger, C. Mozayan, and S. Rudraraju for assistance with sample preparation and measurements; and F. Göktepe and Ö. Göktepe for valuable discussions. Support is largely from Air Force Office of Scientific Research grants FA9550-09-1-0537 and FA9550-12-1-0211, with additional support from Office of Naval Research MURI grant N00014-08-1-0654, Robert A. Welch Foundation grant AT-0029, the Creative Research Initiative Center for Bio-Artificial Muscle and the Korea–U.S. Air Force Cooperation Program grant-2012-00074 (Korea), and the Centre of Excellence funding from the Australian Research Council. N.L. and Y.C. acknowledge financial support from MoST (grant 2012CB933401) and National Natural Science Foundation of China (grant 50933003). D.S.G., L.D.M., and A.F.F. are research fellows of the Conselho Nacional de Desenvolvimento Científico e Tecnológico and the Fundação de Amparo à Pesquisa do Estado de São Paulo of Brazil. A provisional patent application on the topic of this manuscript has been filed by N. Li *et al.*, "Coiled and non-coiled nanofiber yarn torsional and tensile actuators," U.S. Provisional Patent 61678340 (1 August 2012).

Supplementary Materials

www.sciencemag.org/cgi/content/full/338/6109/928/DC1
Supplementary Text
Figs. S1 to S11
References (*33*–*37*)
Movies S1 to S5

2 July 2012; accepted 13 September 2012
10.1126/science.1226762

REPORTS

Synthetic Lipid Membrane Channels Formed by Designed DNA Nanostructures

Martin Langecker,[1]* Vera Arnaut,[1]* Thomas G. Martin,[2]* Jonathan List,[1] Stephan Renner,[1] Michael Mayer,[3] Hendrik Dietz,[2]† Friedrich C. Simmel[1]†

We created nanometer-scale transmembrane channels in lipid bilayers by means of self-assembled DNA-based nanostructures. Scaffolded DNA origami was used to create a stem that penetrated and spanned a lipid membrane, as well as a barrel-shaped cap that adhered to the membrane, in part via 26 cholesterol moieties. In single-channel electrophysiological measurements, we found similarities to the response of natural ion channels, such as conductances on the order of 1 nanosiemens and channel gating. More pronounced gating was seen for mutations in which a single DNA strand of the stem protruded into the channel. Single-molecule translocation experiments show that the synthetic channels can be used to discriminate single DNA molecules.

A large class of proteins and peptides form channels through lipid bilayer membranes (*1*) to facilitate the transport of water, ions, or other entities through the otherwise impermeable membranes. Here, we report on a synthetic membrane channel that is constructed entirely from DNA and anchored to a lipid membrane by cholesterol side chains. The shape of our synthetic channel is inspired by the natural channel protein α-hemolysin (*2*), although there are differences in physical properties such as charge, hydrophobicity, and size.

We constructed the channel by means of molecular self-assembly with scaffolded DNA origami (*3*–*9*) (Fig. 1A). The channel consists of two modules: (i) a stem that penetrates and spans a lipid membrane, and (ii) a barrel-shaped cap

[1]Lehrstuhl für Bioelektronik, Physics Department and ZNN/WSI, Technische Universität München, 85748 Garching, Germany. [2]Walter Schottky Institute, Physics Department, Technische Universität München, 85748 Garching, Germany. [3]Department of Biomedical Engineering, University of Michigan, Ann Arbor, MI 48109, USA.

*These authors contributed equally to this work.
†To whom correspondence should be addressed. E-mail: dietz@tum.de (H.D.); simmel@tum.de (F.C.S.)

that adheres to the cis side of the membrane. Adhesion to the lipid bilayer is mediated by 26 cholesterol moieties that are attached to the cis-facing surface of the barrel (Fig. 1A). The stem protrudes centrally from the barrel and consists of six double-helical DNA domains that form a hollow tube. The interior of this tube acts as a transmembrane channel, with a diameter of ~2 nm and a length of ~42 nm, that runs through both stem and barrel (Fig. 1, B and C).

Transmission electron microscopy (TEM) images taken from purified structures (Fig. 1D) confirmed that the intended shape is realized (text S1 and figs. S1 and S2) (*10*). Experiments with unilamellar lipid vesicles show that the synthetic DNA channels bind to lipid bilayer membranes (Fig. 1, E to G, text S2, and figs. S4 to S8) in the desired orientation in which the cholesterol-modified face of the barrel forms a tight contact with the membrane and the stem appears to protrude into the lipid bilayer (Fig. 1F and fig. S9).

These observations suggested that the synthetic DNA channels could form membrane pores as designed. Because the energetic cost for insertion of the charged DNA structure into the hydrophobic core of the lipid membrane would be prohibitively high, membrane penetration is thought to involve reorganization of the lipid bilayer around the charged stem structure, with the hydrophilic lipid head groups oriented toward the DNA structure (see text S3).

To demonstrate the electrical conductivity of the resulting membrane pores, we performed single-channel electrophysiological experiments (*11*) using an integrated chip-based setup (fig. S14) (*12*). We added synthetic DNA channels at low concentrations (~200 pM) to the cis side of the setup and applied voltage pulses to facilitate

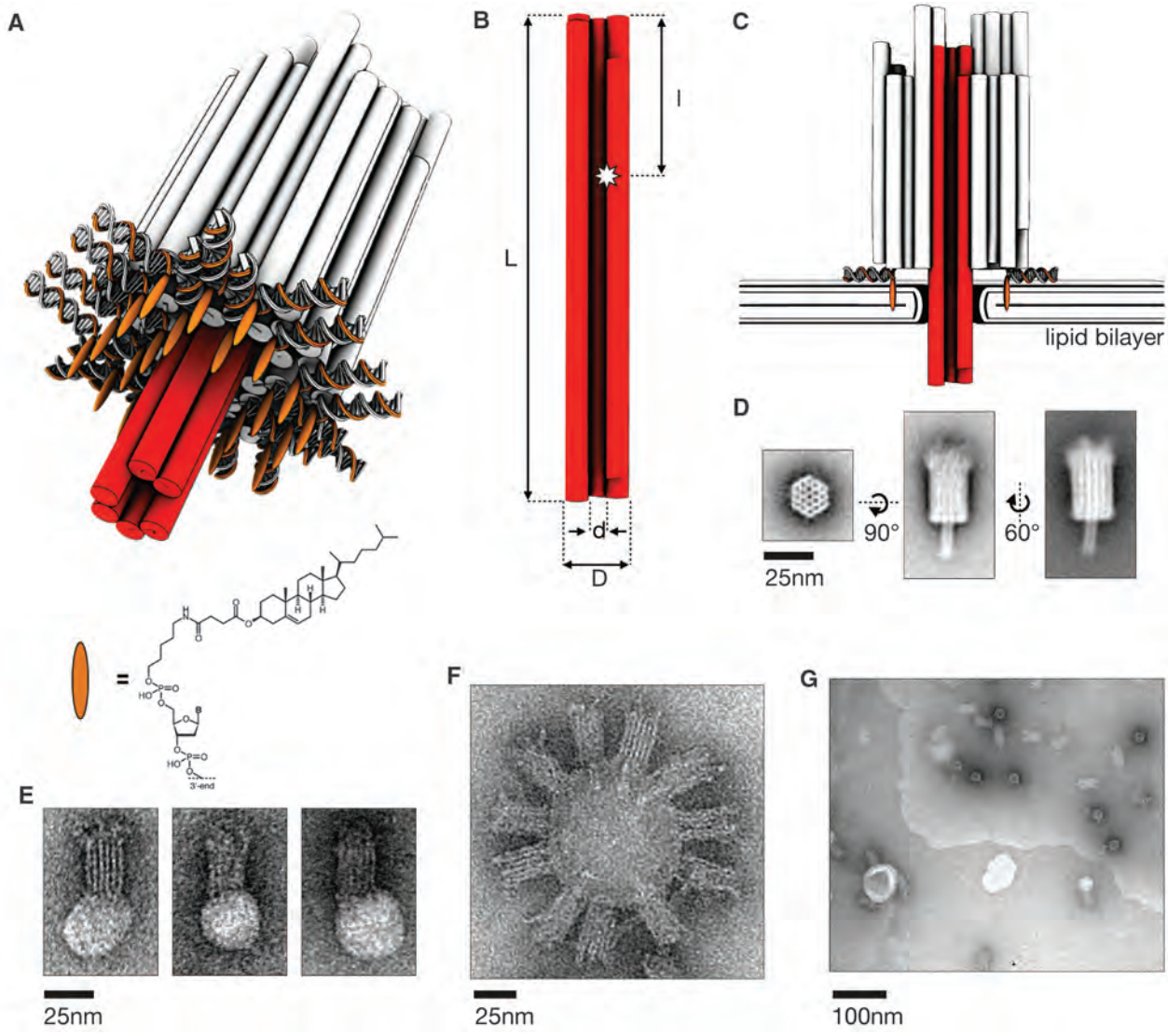

Fig. 1. Synthetic DNA membrane channels. (**A**) Schematic illustration of the channel formed by 54 double-helical DNA domains packed on a honeycomb lattice. Cylinders indicate double-helical DNA domains. Red denotes transmembrane stem; orange strands with orange ellipsoids indicate cholesterol-modified oligonucleotides that hybridize to single-stranded DNA adaptor strands. (**B**) Geometric specifications of the transmembrane channel. Length L = 47 nm, tube diameter D = 6 nm, inner diameter d = 2 nm. The length of the central channel fully surrounded by DNA helices is 42 nm. The star symbol indicates the position of a 7-base strand extension acting as a "defect" in channel "mutants" [l = 15 nm for mutant M1 and l = 14 nm for mutant M2; see text S6 and caDNAno maps (figs. S22 to S24)]. (**C**) Cross-sectional view through the channel when incorporated in a lipid bilayer. (**D**) Averaged negative-stain TEM images obtained from purified DNA channel structures (class averages obtained from raw images displayed in figs. S1 and S2). (**E** and **F**) Example TEM images of DNA channels adhering to small unilamellar vesicles (SUVs) made from POPC (1-palmitoyl-2-oleoyl-*sn*-glycero-3-phosphocholine) lipids. More images and a statistical analysis of vesicle size distribution and binding efficiency are found in text S2 and figs. S4 to S9. (**G**) TEM image of DNA channels binding to an extended lipid bilayer in the upper right part of the image. DNA channels are found predominantly on lipid-covered areas or sticking to SUVs (see text S2).

incorporation into the membrane (*13*, *14*) (fig. S11A). As with biological channels, successful membrane incorporation of individual synthetic DNA channels manifested itself in a stepwise increase in transmembrane current (Fig. 2A) along with an increase in electrical noise (fig. S11B). Depending on the preparation method, we also observed incorporation of multiple DNA channels into the same membrane (fig. S13). The synthetic DNA channels displayed an average ohmic conductance of $G = 0.87 \pm 0.15$ nS (ionic current $I = 174$ pA at 200 mV) per channel in a solution containing 1 M KCl and 2 mM $MgCl_2$ (Fig. 2, B and C). A simple geometrical model (*1*) predicts $G = 0.78$ nS for a channel with diameter of 2 nm and length of 42 nm (text S4), which agrees favorably with what we observe.

Many natural ion channels display current gating caused by switching between distinct channel conformations with different conductances (*1*). The synthetic DNA channels also displayed gating behavior (Fig. 2D, traces i to iii), which may be caused by thermal fluctuations of the structure. We hypothesized that stochastic unzipping and rezipping of short double-helical DNA domains in the channel may also contribute to the observed current gating. To test this idea, we designed three channel "mutants" that differed from the "wild-type" channel only by a single-stranded heptanucleotide protruding from the central transmembrane tube (Fig. 1B and text S6). The mutant channels showed more pronounced gating than did wild-type channels (Fig. 2D, traces iv to vi), and they also significantly differed in their gating time statistics (Fig. 2E and fig. S16). Every investigated mutant channel displayed gating, whereas some of the wild-type channels did not show gating at all (Fig. 2D, trace i). Hence, the transmembrane current depended on fine structural details of the synthetic DNA channel.

In the past, nanoscale membrane pores have shown great potential for use as single-molecule biosensors (*15*–*22*), whose operation principle is based on the transient blockage of ionic current by analyte molecules. The type of sensing task that can be accomplished with such "nanopores" depends on their size and their chemical structure. Nanopore sensors based on naturally occurring membrane pores provide excellent electrical properties, but altering the geometry of biological pores and introducing chemical functions through genetic engineering or chemical conjugation is challenging. By contrast, the geometry of synthetic DNA objects (*23*, *24*) and their chemical properties (*24*) can be tailored for custom nanopore sensing applications. Here, we used our synthetic DNA lipid membrane channel for single-molecule studies of DNA hairpin unzipping and guanine quadruplex (*25*) unfolding. Single-stranded DNA is expected to fit through the 2-nm central pore of the DNA channel, whereas larger DNA secondary structures such as hairpins or quadruplexes are not (*26*, *27*). To translocate through the DNA channel, the structures must unzip or unfold as in similar experiments with α-hemolysin, thus providing a characteristic time delay in the current blockades that reveals the kinetics of structural transitions (*26*–*28*).

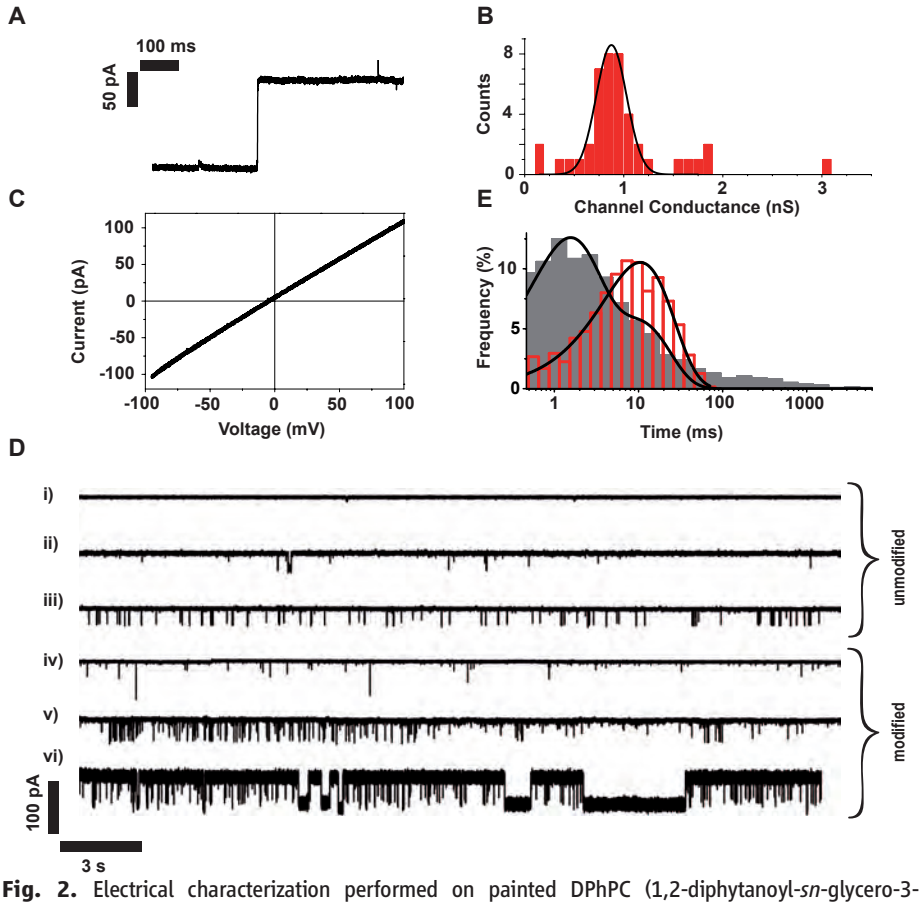

Fig. 2. Electrical characterization performed on painted DPhPC (1,2-diphytanoyl-*sn*-glycero-3-phosphocholine) bilayers on a chip-based electrophysiology setup (an Ionera MECA-16 chip on a Nanion Orbit platform). (**A**) Stepwise increase in ionic current during an incorporation event at $V = 200$ mV. (**B**) Histogram of channel conductances obtained from 43 incorporation events. The black line depicts a Gaussian fit. (**C**) Current-voltage dependence of the channel after incorporation. (**D**) Typical current traces obtained from "wild-type" channels (i to iii) and "mutants" with modification M2 (iv to vi) (see text S6). (**E**) Statistics of gating times for the wild-type (red) and mutant (gray) channels. Continuous lines correspond to a monoexponential fit for the wild-type channel ($\tau = 10.5$ ms) and a double-exponential fit for the mutant ($\tau_1 = 1.3$ ms, $\tau_2 = 9.2$ ms).

For one set of experiments, we used a DNA hairpin with a 9–base pair stem flanked by 50 thymidines on the 3′ end and 6 thymidines on the 5′ end (Fig. 3A). The hairpin molecules were initially added to the cis side of a lipid membrane containing a single synthetic DNA channel that displayed a stable current baseline without gating. Application of a positive voltage bias led to capture, unzipping, and translocation of the hairpin structures, resulting in transient current blockades (Fig. 3, A and B). Reversal of the bias after ~30 min again led to transient current blockades, this time caused by molecules that had accumulated in the trans compartment by previous translocation through the DNA channel. The blockade amplitudes for both translocation directions were $\Delta I_{cis\text{-}trans} = 11.9 \pm 2.7$ pA and $\Delta I_{trans\text{-}cis} = 20.3 \pm 4.2$ pA. The blockade dwell times were distributed exponentially, with a characteristic lifetime of $\tau_{cis\text{-}trans} = 1.5$ ms and $\tau_{trans\text{-}cis} = 1$ ms, respectively (Fig. 3C).

In another set of experiments, we added quadruplex-forming oligonucleotides with a single-stranded tail consisting of 60 thymidines (Q-T60) to the cis side of a membrane containing a single synthetic DNA channel (Fig. 3, D and E). Again we observed transient current blockades, which correspond to the capture and threading of quadruplex DNA molecules into the channel, followed by unfolding and subsequent translocation through the pore. Removal of the analyte from the cis compartment restored a stable baseline current without blockades. Subsequent addition of quadruplex DNA with a longer 125-deoxythymidine (dT) tail (Q-T125) led to larger current blockades. The average current blockades were $\Delta I_{Q\text{-}T60} = 5.6 \pm 1.0$ pA and $\Delta I_{Q\text{-}T125} = 15.3 \pm 2.3$ pA, respectively. The larger current blockade for Q-T125 relative to Q-T60 translocations can be explained by the larger volume occupied in the channel by the longer T_{125} tail than by the T_{60} tail (text S7). The blockade dwell times were distributed

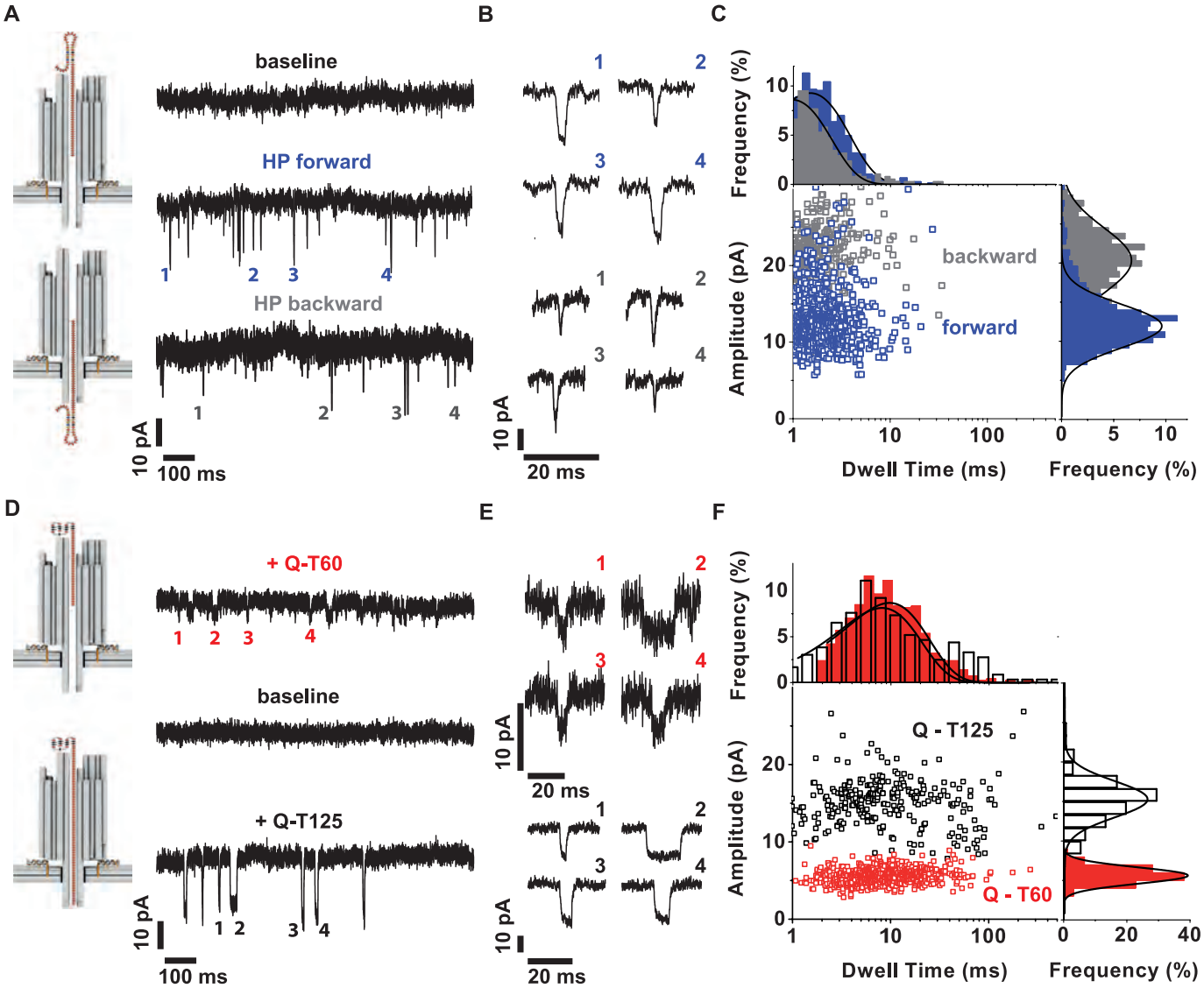

Fig. 3. DNA translocation studies. (**A**) Addition of DNA hairpins (T5-HP-T50) to a DNA channel at V = 200 mV results in the appearance of current blockades, indicating unzipping and translocation of hairpin molecules from cis to trans. Hairpins accumulated on the trans side can also be transferred back from trans to cis by a reversal of the transmembrane voltage. (**B**) Representative blockade events for forward (top) and backward (bottom) translocation of DNA hairpins. (**C**) Scatterplot for the translocation of T5-HP-T50 DNA through a DNA channel from cis to trans (blue) and from trans to cis side (gray) at V = 200 mV, and corresponding histograms. Each data point corresponds to a single translocation event. In total, 777 forward and 379 backward events were analyzed. (**D**) Top: Typical current trace at V = 200 mV after addition of 10 μM Q-T60 DNA. Middle: Current trace after rinsing with buffer solution. Bottom: Current trace after subsequent addition of 10 μM Q-T125 DNA to the same channel. (**E**) Representative blockade events for Q-T60 DNA (top) and Q-T125 DNA (bottom). (**F**) Scatterplot of current blockade versus dwell time for the translocation of Q-T60 DNA (red) and Q-T125 DNA (black) through the DNA channel. In total, 631 Q-T60 events and 279 Q-T125 events were analyzed; corresponding histograms are shown; the lines correspond to single-exponential fits (top histogram) and Gaussian fits (right histograms).

exponentially, with characteristic lifetimes of $\tau_{Q\text{-}T60}$ = 9.7 ms and $\tau_{Q\text{-}T125}$ = 8.1 ms. Thus, like biological pores, our synthetic DNA channels can be used as sensing devices to discriminate analyte molecules by studying their translocation characteristics.

In addition to single-molecule sensing, the synthetic DNA channels introduced here open up broad perspectives for applications as antimicrobial agents and interference with cellular homeostasis. More generally, we believe that fully synthetic lipid membrane channels are a crucial first step toward harnessing ion flux for driving sophisticated nanodevices inspired by the rich functional diversity of natural membrane machines, such as ion pumps, rotary motors, and transport proteins.

References and Notes

1. B. Hille, *Ion Channels of Excitable Membranes* (Sinauer, Sunderland, MA, ed. 3, 2001).
2. L. Song *et al.*, *Science* **274**, 1859 (1996).
3. P. W. K. Rothemund, *Nature* **440**, 297 (2006).
4. S. M. Douglas *et al.*, *Nature* **459**, 414 (2009).
5. E. S. Andersen *et al.*, *Nature* **459**, 73 (2009).
6. H. Dietz, S. M. Douglas, W. M. Shih, *Science* **325**, 725 (2009).
7. N. C. Seeman, *Annu. Rev. Biochem.* **79**, 65 (2010).
8. D. Han *et al.*, *Science* **332**, 342 (2011).
9. C. E. Castro *et al.*, *Nat. Methods* **8**, 221 (2011).
10. See supplementary materials on *Science* Online.
11. B. Sakmann, E. Neher, *Single Channel Recording* (Plenum, New York, 1995).
12. G. Baaken, M. Sondermann, C. Schlemmer, J. Rühe, J. C. Behrends, *Lab Chip* **8**, 938 (2008).
13. C. Danelon, E. M. Nestorovich, M. Winterhalter, M. Ceccarelli, S. M. Bezrukov, *Biophys. J.* **90**, 1617 (2006).
14. S. Renner, A. Bessonov, F. C. Simmel, *Appl. Phys. Lett.* **98**, 083701 (2011).
15. J. J. Kasianowicz, E. Brandin, D. Branton, D. W. Deamer, *Proc. Natl. Acad. Sci. U.S.A.* **93**, 13770 (1996).
16. H. Bayley, P. S. Cremer, *Nature* **413**, 226 (2001).

17. S. Howorka, Z. Siwy, *Chem. Soc. Rev.* **38**, 2360 (2009).
18. C. Dekker, *Nat. Nanotechnol.* **2**, 209 (2007).
19. A. R. Hall *et al.*, *Nat. Nanotechnol.* **5**, 874 (2010).
20. D. Branton *et al.*, *Nat. Biotechnol.* **26**, 1146 (2008).
21. S. Majd *et al.*, *Curr. Opin. Biotechnol.* **21**, 439 (2010).
22. E. A. Manrao *et al.*, *Nat. Biotechnol.* **30**, 349 (2012).
23. N. A. W. Bell *et al.*, *Nano Lett.* **12**, 512 (2012).
24. R. Wei, T. G. Martin, U. Rant, H. Dietz, *Angew. Chem. Int. Ed.* **51**, 4864 (2012).
25. S. Burge, G. N. Parkinson, P. Hazel, A. K. Todd, S. Neidle, *Nucleic Acids Res.* **34**, 5402 (2006).
26. W. Vercoutere *et al.*, *Nat. Biotechnol.* **19**, 248 (2001).
27. A. F. Sauer-Budge, J. A. Nyamwanda, D. K. Lubensky, D. Branton, *Phys. Rev. Lett.* **90**, 238101 (2003).
28. J. Mathé, H. Visram, V. Viasnoff, Y. Rabin, A. Meller, *Biophys. J.* **87**, 3205 (2004).

Acknowledgments: Supported by the Deutsche Forschungsgemeinschaft [grant SFB 863 and Excellence Clusters NIM (Nanosystems Initiative Munich) and CIPSM (Center for Integrated Protein Science Munich)], the Bundesministerium für Bildung und Forschung (grant 13N10970), the European Research Council (starting grant GA 256270, H.D.), the Technische Universität München Institute for Advanced Study, and NIH grant 1R01GM081705 (M.M.). We thank M. Hiller and A. Bessonov for preliminary work, G. Baaken and J. Behrends for kindly providing the MECA chips, and A. Seifert, M. Beckler, and N. Fertig for technical support with the Orbit setup. M.M., H.D., and F.C.S. designed the research; M.L., V.A., and S.R. performed electrophysiological experiments; T.G.M. prepared the synthetic DNA channels and performed TEM; J.L., V.A., and T.G.M. performed experiments with lipid vesicles; and H.D. and F.C.S. wrote the paper. All authors discussed the results and commented on the manuscript.

Supplementary Materials
www.sciencemag.org/cgi/content/full/338/6109/932/DC1
Materials and Methods
Texts S1 to S9
Figs. S1 to S24
Tables S1 to S3
References (*29*–*46*)

4 June 2012; accepted 27 September 2012
10.1126/science.1225624

Coherent Phonon Heat Conduction in Superlattices

Maria N. Luckyanova,[1]* Jivtesh Garg,[1]* Keivan Esfarjani,[1] Adam Jandl,[2] Mayank T. Bulsara,[2] Aaron J. Schmidt,[3] Austin J. Minnich,[4] Shuo Chen,[5] Mildred S. Dresselhaus,[6,7] Zhifeng Ren,[5] Eugene A. Fitzgerald,[2] Gang Chen[1]†

The control of heat conduction through the manipulation of phonons as coherent waves in solids is of fundamental interest and could also be exploited in applications, but coherent heat conduction has not been experimentally confirmed. We report the experimental observation of coherent heat conduction through the use of finite-thickness superlattices with varying numbers of periods. The measured thermal conductivity increased linearly with increasing total superlattice thickness over a temperature range from 30 to 150 kelvin, which is consistent with a coherent phonon heat conduction process. First-principles and Green's function–based simulations further support this coherent transport model. Accessing the coherent heat conduction regime opens a new venue for phonon engineering for an array of applications.

Heat conduction usually occurs by a random walk of thermal energy carriers such as phonons, electrons, or molecules. During the last two decades, size effects on phonon heat conduction that lead to a deviation from this random walk behavior have drawn considerable attention (*1*). Most experimental observations of phonon size effects can be explained by invoking the Casimir picture, wherein phonons travel ballistically or quasi-ballistically through the internal region of the specimen and scatter at interfaces and boundaries (*2*). Such classical size effects are important for a wide range of applications including thermoelectric energy conversion and microelectronic thermal management.

In this classical size regime, the phase information carried by phonons is lost through the diffuse scattering of phonons at boundaries and by internal scattering processes. However, it should be possible to control the conduction of heat by manipulating phonon waves through, for example, stop-band formation in periodic structures (*3*), soliton waves (*4*), and phonon localization (*5*). Such manipulations require that heat-carrying phonons maintain their phase information throughout the heat conduction process. Coherent phonons in superlattices (SLs) have been observed with Raman and acoustic reflection and transmission experiments, but these experiments probe a single frequency (*6*–*8*), rather than the integrated distribution associated with heat transfer. Thus, a conclusive demonstration of coherent phonon heat conduction remains an open challenge.

The term "coherent" has different meanings in different fields. Typically, it is used to characterize the source of a nearly monochromatic wave and implies a measurable phase relationship for a given time interval during wave propagation. Although this definition applies to a monochromatic wave, it does not apply to heat conduction, which involves all the thermally excited phonons in a structure. To clarify the meaning of coherent heat conduction, we consider heat conduction across the thickness of a thin film. In the Casimir classical size effect regime, broadband phonons thermally excited at one boundary traverse the

[1]Department of Mechanical Engineering, Massachusetts Institute of Technology, Cambridge, MA 02139, USA. [2]Department of Materials Science and Engineering, Massachusetts Institute of Technology, Cambridge, MA 02139, USA. [3]Department of Mechanical Engineering, Boston University, Boston, MA 02215, USA. [4]Division of Engineering and Applied Science, California Institute of Technology, Pasadena, CA 91125, USA. [5]Department of Physics, Boston College, Chestnut Hill, MA 02467, USA. [6]Department of Physics, Massachusetts Institute of Technology, Cambridge, MA 02139, USA. [7]Department of Electrical Engineering and Computer Science, Massachusetts Institute of Technology, Cambridge, MA 02139, USA.

*These authors contributed equally to this work.
†To whom correspondence should be addressed. E-mail: gchen2@mit.edu

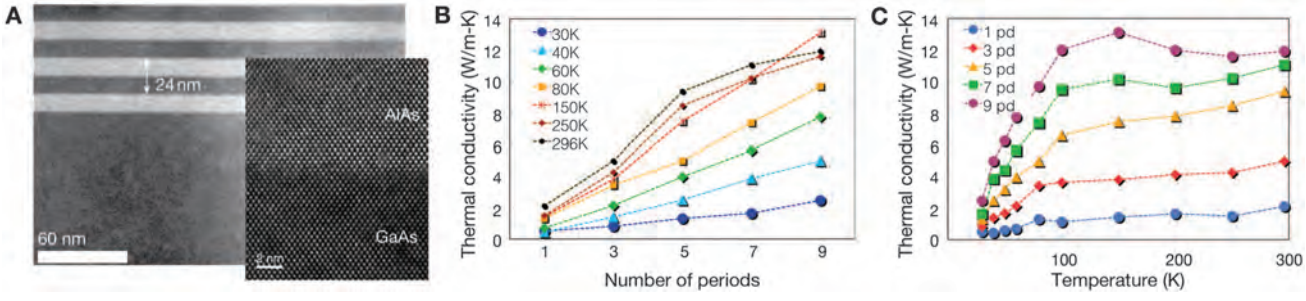

Fig. 1. (**A**) Cross-sectional TEM image of the 3-period (pd) SL. (Inset) HRTEM image of one of the interfaces. Measured thermal conductivity of GaAs/AlAs SLs as a function of (**B**) number of periods in the SL for different temperatures and (**C**) temperature for different SL thicknesses. If the interfaces in the SLs destroy the phonon coherence, the measured thermal conductivity is expected to be independent of the number of periods. Below 150 K, the linearity of the thermal conductivity versus length suggests that phonon heat conduction in these SLs is coherent.